Applied Physics Letters

High mobility and high thermoelectric power factor in epitaxial ScN thin films deposited with plasma-assisted molecular beam epitaxy

Cite as: Appl. Phys. Lett. **116**, 152103 (2020); https://doi.org/10.1063/5.0004761
Submitted: 14 February 2020 . Accepted: 25 March 2020 . Published Online: 14 April 2020

Dheemahi Rao, Bidesh Biswas, Eduardo Flores, Abhijit Chatterjee, Magnus Garbrecht, Yee Rui Koh, Vijay Bhatia, Ashalatha Indiradevi Kamalasanan Pillai, Patrick E. Hopkins, Marisol Martin-Gonzalez, and Bivas Saha

Applied Physics Letters ARTICLE scitation.org/journal/apl

High mobility and high thermoelectric power factor in epitaxial ScN thin films deposited with plasma-assisted molecular beam epitaxy

Cite as: Appl. Phys. Lett. **116**, 152103 (2020); doi: 10.1063/5.0004761
Submitted: 14 February 2020 · Accepted: 25 March 2020 ·
Published Online: 14 April 2020

View Online Export Citation CrossMark

Dheemahi Rao,[1,2,3] Bidesh Biswas,[1,2,3] Eduardo Flores,[4] Abhijit Chatterjee,[1,2,3] Magnus Garbrecht,[5] Yee Rui Koh,[6] Vijay Bhatia,[5] Ashalatha Indiradevi Kamalasanan Pillai,[5] Patrick E. Hopkins,[6,7,8] Marisol Martin-Gonzalez,[4] and Bivas Saha[1,2,3,a)]

AFFILIATIONS

[1]Chemistry and Physics of Materials Unit, Jawaharlal Nehru Centre for Advanced Scientific Research, Bangalore 560064, India
[2]International Centre for Materials Science, Jawaharlal Nehru Centre for Advanced Scientific Research, Bangalore 560064, India
[3]School of Advanced Materials, Jawaharlal Nehru Centre for Advanced Scientific Research, Bangalore 560064, India
[4]Instituto de Micro and Nanotecnologia, IMN-CSIC, C/Isaac Newton 8, Tres Cantos, 28760 Madrid, Spain
[5]Australian Centre for Microscopy and Microanalysis, The University of Sydney, Camperdown, NSW 2006, Australia
[6]Department of Mechanical and Aerospace Engineering, University of Virginia, Charlottesville, Virginia 22904, USA
[7]Department of Materials Science and Engineering, University of Virginia, Charlottesville, Virginia 22904, USA
[8]Department of Physics, University of Virginia, Charlottesville, Virginia 22904, USA

[a)]**Author to whom correspondence should be addressed:** bsaha@jncasr.ac.in and bivas.mat@gmail.com

ABSTRACT

Scandium nitride (ScN) is an emerging rock salt III-nitride semiconductor and has attracted significant interest in recent years for its potential thermoelectric applications as a substrate for high-quality epitaxial GaN growth and as a semiconducting component for epitaxial single-crystalline metal/semiconductor superlattices for thermionic energy conversion. Solid-solution alloys of ScN with traditional III-nitrides such as $Al_xSc_{1-x}N$ have demonstrated piezoelectric and ferroelectric properties and are actively researched for device applications. While most of these exciting developments in ScN research have employed films deposited using low-vacuum methods such as magnetron sputtering and physical and chemical vapor depositions for thermoelectric applications and Schottky barrier-based thermionic energy conversion, it is necessary and important to avoid impurities, tune the carrier concentrations, and achieve high-mobility in epitaxial films. Here, we report the high-mobility and high-thermoelectric power factor in epitaxial ScN thin films deposited on MgO substrates by plasma-assisted molecular beam epitaxy. Microstructural characterization shows epitaxial 002 oriented ScN film growth on MgO (001) substrates. Electrical measurements demonstrated a high room-temperature mobility of 127 $cm^2/V\,s$ and temperature-dependent mobility in the temperature range of 50–400 K that is dominated by dislocation and grain boundary scattering. High mobility in ScN films leads to large Seebeck coefficients ($-175\,\mu V/K$ at 950 K) and, along with a moderately high electrical conductivity, a large thermoelectric power factor (2.3×10^{-3} $W/m\text{-}K^2$ at 500 K) was achieved, which makes ScN a promising candidate for thermoelectric applications. The thermal conductivity of the films, however, was found to be a bit large, which resulted in a maximum *figure-of-merit* of 0.17 at 500 K.

Transition metal nitrides (TMNs) are an interesting class of materials and have attracted significant interest in recent years for a range of energy conversion applications such as solar-thermophotovoltaics (STPVs),[1] photo-catalysis,[2] thermoelectrics,[3–5] and thermionic energy conversion.[6,7] Scandium nitride (ScN) is the most famous semiconducting TMN and exhibits corrosion-resistant high mechanical hardness (~21 GPa),[8] structural, morphologic, and thermodynamic stabilities,[9] and large melting temperatures in excess of 2600 °C.[10,11] Unlike the other traditional wurtzite III-nitride semiconductors such as GaN and InN, ScN crystallizes in the rock salt structure with octahedral bonding coordination[12,13] and exhibits an indirect bandgap of ~0.9 eV and a direct gap of 2.2 eV.[14–16] Due to its cubic (rock salt) crystal structure and low bandgap, ScN has been utilized in the development of the first epitaxial rock salt

single-crystalline ZrN/ScN[17,18] and TiN/(Al,Sc)N)[19–21] metal/semiconductor multilayers and superlattices, respectively, for Schottky diode-based thermionic energy conversion. ScN has also attracted significant interest from thermoelectric research communities as it exhibits a large thermoelectric power factor ($S^2\sigma$) (S and σ are the Seebeck coefficient and electrical conductivity, respectively) due to the high Seebeck coefficient and moderately high electrical conductivity resulting from its degenerate semiconducting nature. Sputter-deposited ScN thin films on MgO and sapphire substrates have shown a large thermoelectric power factor of $\sim 3.3 \times 10^{-3}$ W/m-K^2 in the temperature range of 500–800 K, which is higher than that of many well-known thermoelectric materials such as Bi_2Te_3 in the same temperature range.[4,22]

In addition to their thermoelectric properties, solid-solution alloys of ScN with other III-nitride semiconductors such as GaN[23] have attracted interest for band structure engineering of GaN-based light-emitting diodes (LEDs) with a reduced indium content and for achieving green LEDs with all nitride semiconductors.[24] Moreover, since the lattice constant of ScN ($a = 4.50$ Å)[16] and the in-plane lattice parameter of GaN ($a = 3.18$ Å)[25] result in a small 0.1% mismatch for the (0001) oriented GaN growth on (111) ScN surfaces, ScN has been utilized as a substrate for reducing the threading dislocation densities in GaN epilayers.[26,27] Wurtzite $Al_xSc_{1-x}N$ solid-solution alloys have exhibited a large *c*-axis piezoelectric coefficient that is higher than that of AlN, and it is currently researched for the development of bulk and surface acoustic devices.[28] Recently, $Al_xSc_{1-x}N$ has also demonstrated ferroelectricity with a continuous distortion of the wurtzite structure to a layered hexagonal phase with the increasing scandium concentration and a ferroelectric-to-paraelectric transition temperature higher than 600 °C.[29] Wurtzite $Al_xSc_{1-x}N$ has also shown promise for high-power electronic and optoelectronic device applications.[30]

Sputter-deposited ScN possesses a high *n*-type carrier concentration of (1–5) $\times 10^{20}$ cm^{-3} due to the presence of unwanted impurities such as oxygen (O_N) and fluorine (F_N), which arise primarily from the source material contaminations and from the large background pressure of O_2, CO_2, CO, H_2O, etc. during the sputtering process and possible nitrogen vacancies (V_N).[3,4] Previous reports of chemical vapor deposited ScN also contained halogen and other impurities arising from the reactants and other sources.[31,32] Hole doped *p*-type ScN films have been developed by incorporating Mg_xN_y inside ScN by magnetron sputtering.[33] The *p*-type ScN:Mg thin film also exhibited high Seebeck coefficients and large thermoelectric power factors at high temperatures.[34] Synchrotron-based x-ray absorption and photoemission measurements have demonstrated a rigid-band electronic structure of ScN across the *n*-type (the presence of unwanted O_N) to *p*-type (intentional Mg_{Sc} hole doping) carrier transition regime, which results in the high Seebeck coefficient and thermoelectric power factor over the transition regime.[35] In short, ScN has attracted great interest in recent years and could lead to several industrial applications in the near future.

While these interesting developments in ScN research over the last five-to-ten years are promising, most of the ScN thin films are deposited by low-vacuum magnetron sputtering, physical and chemical vapor deposition, vapor phase epitaxy methods, etc., where it is extremely challenging to control the impurity concentrations and achieve high crystalline quality.[36,37] Moreover, for electronic, optoelectronic, and thermoelectric applications, it is important to achieve lower carrier concentrations and higher mobility simultaneously and reproducibly. For example, in ScN Schottky diodes, the carrier concentration needs to be reduced to less than 10^{18} cm^{-3} without altering its electron affinity, bandgap, and surface properties. Similarly, in ScN-based metal/semiconductor superlattice heterostructures, lower carrier concentrations are essential for achieving thermionic energy conversion devices. In this regard, ultra-high vacuum molecular beam epitaxy (MBE) should be suitable for high-quality ScN growth and for controlling the impurity and dopant concentrations. MBE growth of high quality ScN and demonstration of interesting properties are also important for its integration with GaN, InN, etc. for various applications. Unfortunately, only a few reports on the ScN depositions by MBE focus primarily on the growth and structural aspects[38–43] with no reports on its thermoelectric properties. Given such a background and with a motivation to eventually develop ScN-based Schottky diodes and metal/semiconductor superlattice-based thermionic energy converters, in this Letter, growth and structural characterization of ScN epilayers deposited by plasma-assisted molecular beam epitaxy (PAMBE) in an ultrahigh vacuum environment are demonstrated alongside its impressive thermoelectric properties. In particular, high-mobility and high-thermoelectric power factors in ScN films have been achieved and the physical mechanism of such transport properties is discussed, which will make it attractive for waste heat to electrical energy conversion applications.

ScN thin films with varying thicknesses are deposited by PAMBE inside an ultra-high vacuum chamber with a base pressure of 2×10^{-10} Torr on the (001) MgO substrate at a growth temperature of 600 °C. High purity Sc (99.95% TREM) and N_2 (99.99999%) gas are used for the depositions, and a scandium K-cell temperature of 1320 °C is used to achieve the desired Sc beam equivalent pressure (BMP) of 1×10^{-7} Torr. The N_2 flow rate was kept constant at 1.2 sccm with a forward rf-power of 375 W. It is important to note that the Sc MBE source contained 500 ppm oxygen that is a known *n*-type dopant inside ScN. Except for the presence of oxygen, no other elements have a substantial presence in the source material. Further details about the growth process, deposition rate, etc. are presented in the supplementary material.

Post-growth structural characterization of ScN films using symmetric x-ray diffraction analysis show (002) oriented ScN crystal growth on (001) MgO substrates [see Fig. 1(a) for a representative spectrum of the 600 nm thick film]. The main 002 diffraction peak was located at 39.9°, which results in a ScN lattice constant of 4.51 Å, which is consistent with previous literature reports.[38,42] The MgO

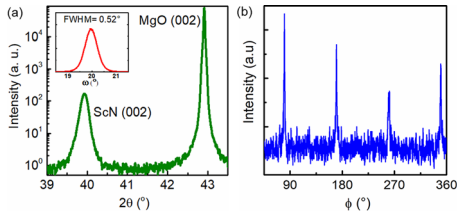

FIG. 1. (a) Symmetric 2θ-ω x-ray diffraction spectrum of ScN deposited on the MgO substrate. ScN grows with 002 orientations on the (001) MgO substrate with a small FWHM of the rocking curve of 0.52° (shown in the inset). (b) Asymmetric φ-scan of ScN that shows four equally spaced peaks representative of its epitaxial crystal growth.

substrate 002 diffraction maxima were also found at 42.9°, representing its lattice constant of 4.21 Å, as expected.[44] The full-width-at-the-half-maxima (FWHM) of the rocking curve (ω-scan) corresponding to the main 002 peak was found to be 0.52° in ScN, which is indicative of epitaxial and textured film growth on MgO substrates. The FWHM of the rocking curve is consistent with the previous reports of ScN growth by radical-source MBE[40] and is generally significantly smaller than that of the sputter-deposited films that exhibit much higher FWHM values between ∼1° and 1.5° depending on the growth conditions such as substrate temperature.[14] Four equally spaced asymmetric ScN 111 φ-peaks that are separated by 90° apart from each other [see Fig. 1(b)] represents epitaxial ScN film growth on MgO substrates.

High-resolution (scanning)/transmission electron microscopy (HR(S)/TEM) analysis of the as-deposited ScN film reveals [see Fig. 2(a)] pyramidal grain growth with an epitaxial relationship of [001](001) ScN || [001](001) MgO substrates within the grains. The pyramids are separated by inverted pyramid-like structures with grain boundaries that though maintains the out-of-plane epitaxy, but rotates the grain along the in-plane directions [see Fig. 1(a) in the supplementary material]. The inverted pyramid structures grow at a slightly faster rate and represent themselves as plateau-pyramid structures in the plan-view scanning electron microscopy (SEM) [see Fig. 3(a)] and atomic force microscopy (AFM) images [see Fig. 1(b) in the supplementary material]. It is important to note here that although no detailed HR(S)/TEM based microscopy analysis was performed in previous MBE growth of ScN on MgO substrates, previous AFM images had exhibited similar plateau-pyramid structures found here.[38,42] The SEM images reveal flatter top surfaces with a root mean square (RMS) surface roughness of 1.13 nm, measured using AFM. Along with the pyramidal grains, dislocation networks and stacking faults were also seen in both the pyramidal and inverted pyramid-like regions [see Fig. 2(a)]. (HR(S)/TEM) energy-dispersive spectroscopy (EDS) elemental maps clearly show that Sc and N atoms are uniformly distributed through the film, except along the grain boundary and dislocation lines that are dominated by oxygen atoms. Such a higher concentration of oxygen distribution along the defect lines most likely would have occurred due to the post-growth oxygen diffusion process.

Atomic-resolution HAADF-STEM images [see Fig. 3(b)] clearly show lattice fringes with cube-on-cube epitaxial growth as well as an atomically sharp and abrupt ScN/MgO interface. Due to an ∼6% lattice-mismatch between the ScN and MgO substrates, misfit-dislocations are observed in the STEM images. A detailed discussion on the origin and dynamics of extended defects such as grain boundaries and stacking faults including the effects of growth temperature is beyond the scope of the present study and will be presented later.

To gain an insight into the electronic properties of the MBE deposited ScN thin films, temperature-dependent Hall measurements are performed. At room temperature, the ScN film having a thickness of 450 nm exhibited the highest mobility of 127 $cm^2/V\,s$, with an associated n-type (electron) concentration of $8.6 \times 10^{19}\,cm^{-3}$, which resulted in a room-temperature electrical conductivity of 1759 Scm^{-1}. Such a high mobility obtained in PAMBE-deposited ScN is consistent with the previous reports[4,40,48–52] of ScN growth by radical source MBE and is higher than the mobility obtained with previous sputter-deposited ScN (see Table I in supplementary material). It is important to note here that the measured mobility is high despite the presence of extended defects such as grain boundaries and dislocation networks

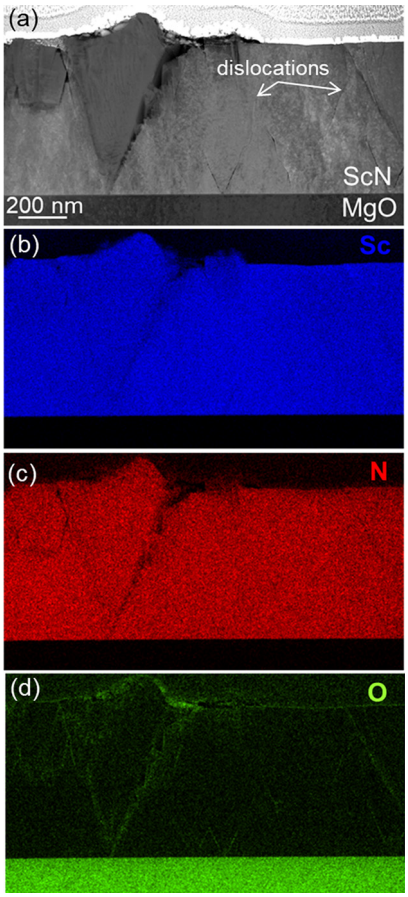

FIG. 2. (a) High-angle annular dark-field scanning transmission electron microscopy (HAADF-STEM) image of ScN deposited on the MgO substrate. An inverted pyramidal grain without the $[001]_{ScN}||[001]_{MgO}$ orientation relationship is visible in the image. Dislocation lines are also visible in the image as highlighted. HRSTEM-EDX maps show that Sc (b) and N (c) atoms are uniformly distributed over the entire ScN layer except for the grain boundaries. Oxygen (d) was found to cluster around the grain boundaries.

that are known to scatter electrons strongly. Subsequent partial or full removal of such defects should increase the mobility even further. The room temperature electrical conductivity of 1759 Scm^{-1} of ScN is comparable to the electrical conductivity of well-known thermoelectric materials such as Bi_2Te_3 and PbTe.[45–47]

Low temperature (50 K–400 K) Hall measurements exhibited a decrease in the electron mobility from 172 $cm^2/V\,s$ at 50 K to 106 $cm^2/V\,s$ at 400 K. To understand the details of the carrier scattering mechanism, the temperature-dependent mobility is modeled with a combination of ionized impurities ($\mu_{ionized\ impurity}$) as well as dislocation scattering ($\mu_{dislocation}$) of electrons as expressed in the following equation:[53]

$$\frac{1}{\mu_{total}} = \frac{1}{\mu_{ionized\ impurity}} + \frac{1}{\mu_{dislocation}}. \quad (1)$$

The electron mobility increases at low temperatures due to ionized impurity scattering with a functional relationship,

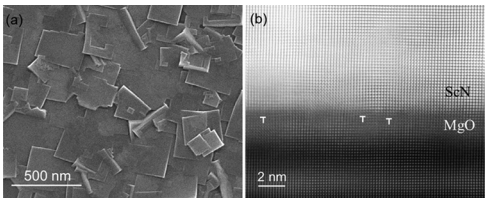

FIG. 3. (a) Plan-view SEM image of ScN showing inverted pyramidal grains growing at a slightly faster rate than the pyramidal grains. Within the grains, the surfaces are very smooth. (b) Atomically sharp and abrupt ScN/MgO interface along with misfit dislocations due to the lattice mismatch between ScN and MgO.

$$\mu_{ionized\ impurity} = AT^{1.5}, \tag{2}$$

where T is the absolute temperature and A is a constant. Dislocations can significantly scatter electrons in semiconductors in two distinct ways, especially when their densities are higher than $10^8\,cm^{-2}$.[53] First, a dislocation can be considered as a line charge and acts as a charged impurity center scattering electrons. Second, the strain field associated with dislocations can act as a scattering center similar to the deformation potential scattering. However, it is well known that the second effect is not appreciable for n-type semiconductors (such as ScN) and influences primarily the p-type materials. Therefore, the dislocation scattering is primarily considered here as a line charge scattering center and expressed as

$$\mu_{dislocation} = \left(\frac{3q}{8N_dR}\right)\frac{1}{(3m^*k_BT)^{0.5}}, \tag{3}$$

where N_d and R are the dislocation density and dislocation core radius, respectively, m^* is the electron effective mass, and q and k_B are the charge of an electron and the Boltzmann constant, respectively. An effective mass of 0.39 m_o ($m_t = 0.28$, $m_l = 2.08$)[33] was used for ScN.

Figure 4(a) shows that the theoretical curve fits the experimental results very well. The fitting also revealed a dislocation core radius of ~1 nm and a high dislocation density of $2 \times 10^{12}\,cm^{-2}$. Although the dislocation density of $\sim 10^{12}\,cm^{-2}$ is quite large, their numbers are quite consistent with the rough estimates from the microscopy analysis. In addition, since the grain boundaries can also act as line charge and scatter electrons, their number densities are also included in the N_d calculation. Temperature-dependent Hall measurements also revealed that carrier densities of ScN exhibit a very small change in the temperature range of 50 K to 400 K [see Fig. 4(b)], suggesting that most dopants are ionized at the lowest temperature of 50 K. Because of the decreasing mobility and relatively unchanged carrier concentration with temperature, the electrical conductivity [see Fig. 4(c)] of the ScN film shows a decrease with increasing temperatures representing its degenerate semiconducting nature.

Since ScN has shown potential for thermoelectric applications before, high-temperature thermoelectric properties such as the Seebeck coefficient and power factor (PF) are measured from 300 K to 950 K. At 400 K, the PAMBE-deposited ScN films exhibit a large Seebeck coefficient of $-107\,\mu V/K$ that is slightly higher than the Seebeck coefficient of previous sputter-deposited ScN of $-95\,\mu V/K$ at the same temperature.[4] With the increase in temperature, the Seebeck coefficient increased monotonically and exhibited a maximum of $-175\,\mu V/K$ at 950 K. Concomitant with the increase in the Seebeck

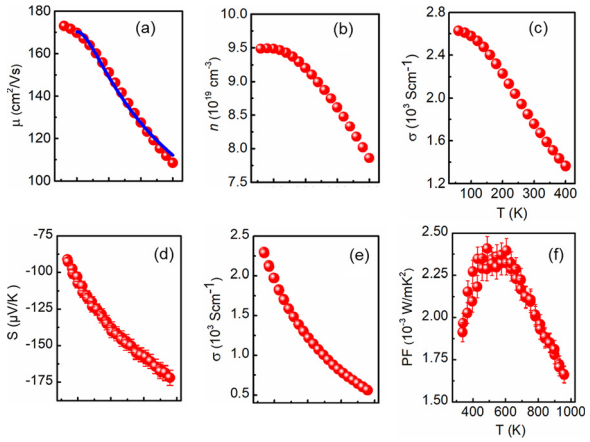

FIG. 4. Low temperature (50 K–400 K) (a) mobility, (b) carrier concentration, and (c) electrical conductivity of the 450 nm ScN thin film. The mobility was found to decrease with increasing temperatures and is fitted with Eq. (1) that accounts for a combination of ionized impurities and the dislocation scattering mechanism (blue line). High temperature (350 K–950 K), (d) Seebeck coefficient, (e) electrical conductivity, and (f) thermoelectric power factor of the PAMBE deposited 300 nm ScN thin film as a function of temperature. ScN films exhibit a maximum thermoelectric power factor of 2.3×10^{-3} W m^{-1} K^{-2} in the temperature range of 500–600 K, which are higher than those of some well-known thermoelectric materials such as Bi_2Te_3.

coefficient, the electrical conductivity of the ScN films decreased from 2.2×10^3 S cm^{-1} at 300 K to $\sim 0.5 \times 10^3$ Scm^{-1} at 950 K. Previous Landauer and Boltzmann transport-based modeling analyses have demonstrated that due to its high carrier concentrations, the Fermi level of ScN is located ~0.06–0.09 eV above the conduction band minima, which leads to the degenerate semiconducting or metallic-like electrical conductivity behavior with increasing temperature.[4]

The thermoelectric power factor ($S^2\sigma$) was found to increase initially in the temperature range of 300 K–600 K, followed by a maximum, and then decreased monotonically [see Fig. 4(f)]. The highest power factor was achieved in the temperature range of 500 K–600 K with a value of $\sim 2.3 \times 10^{-3}$ W m^{-1} K^{-2}, which is comparable with the power factors of previous sputter-deposited ScN,[34] but higher than that of other well-known thermoelectric materials such as La_3Te_4[54] and comparable with the values of high-temperature thermoelectric materials such as SiGe.[55] It is important to note here that in spite of using the UHV-PAMBE method, the power factor of ScN remained comparable to that of sputter-deposited films because of the prsence of oxygen in the Sc source, which resulted in a high carrier concentration. Therefore, efforts should be made to use higher-purity Sc sources or to reduce the carrier concentration by hole doping without altering other electronic properties.

In spite of such a high power factor, the overall thermoelectric *figure-of-merit* (ZT) of ScN was found to be rather low (maximum ZT of 0.17 @ 500 K) due to its high thermal conductivity measured using time domain thermoreflectance (see the supplementary material for details). The thermal conductivity of a 450 nm ScN thin film decreased with increasing temperature due to Umklapp scattering [see Fig. 5(a)] and exhibited an exponent of −1.17. It is important to note that the uncertainty in the thermal conductivity measurement at each temperature was larger than the normal due to the conductivity variations from area-to-area on the surface due to the changes in the surface

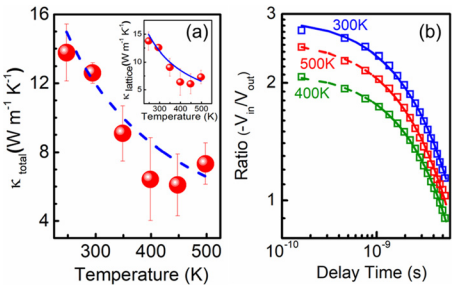

FIG. 5. (a) Total thermal conductivity of the 450 nm ScN thin film measured from 250 K–500 K decreases with increasing temperature due to Umklapp scattering. The dashed line is drawn over the total thermal conductivity as a guide to the eye. (Umklapp model fitting of the lattice contribution to the total thermal conductivity is presented by the blue line in the inset). (b) Time domain thermoreflectance (TDTR) experimental data plotted as the ratio of the in-phase to out-of-phase lock-in voltages as a function of pump-probe delay time and the corresponding model fits used to determine the thermal conductivity of the ScN film. TDTR data are shown for three different measurement temperatures.

morphology resulting from the defects. Nevertheless, fitting of the TDTR data was quite well as exhibited in Fig. 5(b). Further research on alloying or nano-structure formation will be required to reduce the thermal conductivity of ScN without compromising the power factor to obtain higher ZT.

In conclusion, a high mobility of 127 $cm^2/V\,s$ at room temperature and a large thermoelectric power factor of $\sim 2.3 \times 10^{-3}\,W\,m^{-1}\,K^{-2}$ in the temperature range of 500 K–600 K have been achieved in epitaxial ScN thin films deposited by plasma-assisted MBE. The epitaxial ScN films are found to grow with (002) orientations on the (001) MgO substrates with pyramidal grains separated by inverse pyramids and a sharp and abrupt ScN/MgO interface. The low-temperature mobility was dominated by scattering from dislocations and ionized impurities, which revealed a high dislocation density consistent with HRTEM analysis. In spite of the presence of unwanted impurities such as oxygen, which resulted in a large carrier density, ScN films exhibit a high Seebeck coefficient and a high thermoelectric power factor. Although the thermoelectric power factor was found to be appreciably high, the overall ZT was limited to 0.17 due to the high thermal conductivity of 7.3 W/m-K at 500 K. The present work will help attract attention toward ScN for its thermoelectric applications and engineer its structural and material properties for electronic and optoelectronic devices.

See the supplementary material for detailed information related to the growth and the characterization methods.

AUTHORS' CONTRIBUTIONS

D.R. and B.B. contributed equally to this work.
Data are available upon request from the authors.

D.R., B.B., and B.S. acknowledge the International Center for Materials Science (ICMS) and Sheik Saqr Laboratory (SSL) in JNCASR for support. B.S. acknowledges the Science and Engineering Research Board (SERB) of the Government of India, Start-Up Research Grant No. SRG/2019/000613 for financial support. M.S.M.G. wants to acknowledge financial support from No. MAT2017-86450-C4-3-R and intramural CSIC Project No. 2D-MESES. M.G., V.B., and A.I.K.P acknowledge the facilities of Sydney Microscopy and Microanalysis at the University of Sydney. Y.R.K. and P.E.H. appreciate support from a MURI program through the Office of Naval Research, Grant No. N00014-18-1-2429.

REFERENCES

[1]U. Guler, A. Boltasseva, and V. M. Shalaev, Science **344**, 263 (2014).
[2]M. Sakhdari *et al.*, Nano Energy **26**, 371 (2016).
[3]S. Kerdsongpanya *et al.*, Appl. Phys. Lett. **99**, 232113 (2011).
[4]P. V. Burmistrova *et al.*, J. Appl. Phys. **113**, 153704 (2013).
[5]H. Uchiyama *et al.*, Phys. Rev. Lett. **120**, 235901 (2018).
[6]A. Shakouri, Annu. Rev. Mater. Res. **41**, 399 (2011).
[7]J. M. Zide *et al.*, Appl. Phys. Lett. **87**, 112102 (2005).
[8]D. Gall *et al.*, J. Appl. Phys. **84**, 6034 (1998).
[9]H. A. Al-Atabi *et al.*, Appl. Phys. Lett. **113**, 122106 (2018).
[10]P. Eklund, S. Kerdsongpanya, and B. Alling, J. Mater. Chem. C **4**, 3905 (2016).
[11]B. Saha, A. Shakouri, and T. D. Sands, Appl. Phys. Rev. **5**, 021101 (2018).
[12]W. Feng *et al.*, Physica B **405**, 2599 (2010).
[13]N. Takeuchi, Phys. Rev. B **65**, 045204 (2002).
[14]B. Saha *et al.*, J. Appl. Phys. **114**, 063519 (2013).
[15]A. Qteish *et al.*, Phys. Rev. B **74**, 245208 (2006).
[16]B. Saha *et al.*, J. Appl. Phys. **107**, 033715 (2010).
[17]V. Rawat *et al.*, J. Appl. Phys. **105**, 024909 (2009).
[18]M. Garbrecht *et al.*, J. Mater. Sci. **51**, 8250 (2016).
[19]M. Y. Shalaginov *et al.*, Laser Photonics Rev. **9**, 120 (2015).
[20]B. Saha *et al.*, Phys. Status Solidi **252**, 251 (2015).
[21]B. Saha *et al.*, Phys. Rev. B **93**, 045311 (2016).
[22]M. Saleemi *et al.*, J. Mater. Chem. **22**, 725 (2012).
[23]M. A. Moram *et al.*, J. Appl. Phys. **106**, 113533 (2009).
[24]M. E. Little and M. E. Kordesch, Appl. Phys. Lett. **78**, 2891 (2001).
[25]S. Strite, J. Vac. Sci. Technol., B **10**, 1237 (1992).
[26]C. F. Johnston *et al.*, J. Cryst. Growth **311**, 3295 (2009).
[27]M. A. Moram *et al.*, J. Cryst. Growth **308**, 302 (2007).
[28]M. Akiyama *et al.*, Adv. Mater. **21**, 593 (2009).
[29]S. Fichtner *et al.*, J. Appl. Phys. **125**, 114103 (2019).
[30]A. Zukauskaite *et al.*, J. Appl. Phys. **111**, 093527 (2012).
[31]J. P. Dismukes *et al.*, J. Cryst. Growth **9**, 295 (1971).
[32]J. P. Dismukes, W. M. Yim, and V. S. Ban, J. Cryst. Growth **13-14**, 365 (1972).
[33]B. Saha *et al.*, Appl. Phys. Lett. **110**, 252104 (2017).
[34]B. Saha *et al.*, Phys. Rev. B **97**, 085301 (2018).
[35]S. Nayak *et al.*, Phys. Rev. B **99**, 161117 (2019).
[36]J. H. Edgar, T. Bohnen, and P. R. Hageman, J. Cryst. Growth **310**, 1075 (2008).
[37]B. Biswas and B. Saha, Phys. Rev. Mater. **3**, 020301 (2019).
[38]A. R. Smith *et al.*, J. Appl. Phys. **90**, 1809 (2001).
[39]J. L. Hall *et al.*, J. Cryst. Growth **311**, 2054 (2009).
[40]T. Ohgaki *et al.*, J. Appl. Phys. **114**, 093704 (2013).
[41]H. A. Al-Brithen, A. R. Smith, and D. Gall, Phys. Rev. B **70**, 045303 (2004).
[42]H. Al-Brithen and A. R. Smith, Appl. Phys. Lett. **77**, 2485 (2000).
[43]S. W. King, R. F. Davis, and R. J. Nemanich, J. Vac. Sci. Technol., A **32**, 061504 (2014).
[44]R. W. G. Wyckoff, *Crystal Structures*, 1st ed. (Wiley, New York, 1963).
[45]K. T. Kim, K. J. Kim, and G. H. Ha, Electron. Mater. Lett. **6**, 177 (2010).
[46]J. P. Heremans, C. M. Thrush, and D. T. Morelli, Phys. Rev. B **70**, 115334 (2004).
[47]Z. H. Dughaish, Physica B **322**, 205 (2002).
[48]J. Casamento *et al.*, Appl. Phys. Lett. **115**, 172101 (2019).
[49]*Proceedings of the First Symposium on III-V Nitride Materials and Processes*, edited by T. D. Moustakas, J. P. Dismukes, and S. J. Pearton (The Electrochemical Society Inc., Pennington, NJ, 1996), Vol. 96, p. 197.
[50]T. Ohgaki *et al.*, J. Cryst. Growth **476**, 12 (2017).
[51]J. S. Cetnar *et al.*, Appl. Phys. Lett. **113**, 192104 (2018).
[52]Y. Oshima, E. G. Villora, and K. Shimamura, J. Appl. Phys. **115**, 153508 (2014).
[53]S. S. Li, *Physics Semiconductor Electronics* (Springer, New York, 2006).
[54]L. Gao *et al.*, J. Phys. D. Appl. Phys. **45**, 185303 (2012).
[55]H. Takiguchi *et al.*, Mater. Trans. **51**, 878 (2010).